Geophys. J. Int. (2006) **164,** 88–98 doi: 10.1111/j.1365-246X.2005.02837.x

Variation of Rayleigh wave group velocity dispersion and seismic heterogeneity of the Indian crust and uppermost mantle

S. Mitra,[1] K. Priestley,[1] V. K. Gaur,[3,4] S. S. Rai[2] and J. Haines[1]

[1]*Bullard Laboratories, University of Cambridge, UK. E-mail: keith@esc.cam.ac.uk*
[2]*National Geophysical Research Institute, Hyderabad, India*
[3]*Indian Institute of Astrophysics, Bangalore, India*
[4]*Center for Mathematical Modelling and Computer Simulations, Bangalore, India*

Accepted 2005 October 7. Received 2005 September 27; in original form 2005 June 3

SUMMARY

We present group velocity dispersion results from a study of regional fundamental mode Rayleigh waves propagating across the Indian region. 1-D, path-averaged dispersion measurements have been made for 1001 source–receiver paths and these combined to produce tomographic images between 15 and 45 s period. Because of the dense station coverage in peninsular India, these images have substantially higher lateral resolution for this region than is currently available from global and regional group velocity studies. Testing of the group velocity model shows that the average resolution across the region is about 7.5° for the periods used in this study. The tomographic maps demonstrate that while the Indian shield is characterized by high crustal and uppermost-mantle group velocities, comparatively lower velocities exist beneath the Himalaya due to the thickened crust and beneath the Gangetic plains caused by the mollasse sediments and recent alluvium cover in the Himalayan foredeep. Northeastern India north of the Shillong Plateau also displays higher velocities, similar to the south Indian shield, indicative of colder crust beneath the region. The northern Bay of Bengal shows extremely low velocities due to the thick sediment blanket of the Bengal fan. Likewise, the Katawaz Basin in southern Pakistan shows lower velocities that resemble those seen in the Bay of Bengal. The geometry of the velocity contours south of the Katawaz Basin closely matches the prograding Indus fan in the Arabian Sea. Finally, the Tibetan Plateau has lower group velocities compared to the Indian shield at all periods as a result of the thick crust beneath southern Tibet.

Key words: group velocity, India, tomography.

1 INTRODUCTION

The Indian region has had a long history of craton assimilations and suffered protracted tectonism in the Phanerozoic, resulting in a wide range of geological realms. India is largely composed of the Precambrian Indian shield and the Himalayan Fold and Thrust belt, which marks its northern collision boundary with Tibet. The continued underthrusting of India beneath Tibet has flexed the lithosphere down immediately south of the Himalaya to form an intervening foredeep filled with several kilometres of sediments. The shield is a collage of cratons and intervening mobile belts assembled between the mid-Archean and neo-Proterozoic time (Naqvi & Rogers 1987), and carved into a peninsula by south-tapering passive continental margins that are covered by a thin veneer of Phanerozoic sediments. A superficially separated northeastern part of the shield is exposed over the Shillong Plateau and Mikir Hills and underlies the foredeep in the region. The sediments derived from the Himalaya and transported seawards by the Ganges and Brahmaputra Rivers are deposited in the Bengal delta covering the floor of the Bay of Bengal (Curray *et al.* 1982) forming the world's largest delta-fan sequence. An analogous Indus fan derived from the western drainage of the Himalaya, albeit of smaller extent, similarly overlays the Arabian Seafloor on the northwestern boundary of the continent.

In this work, we investigate lateral heterogeneity in the crust and uppermost-mantle structure of India and the surrounding region (Fig. 1) using fundamental mode Rayleigh wave group velocity dispersion measurements made on a regional scale. We calculate 1-D path-averaged group velocity dispersion curves for 1001 paths and combine these measurements to produce group velocity tomographic images at a number of periods for India and the surrounding region. We use seismograms from a relatively dense network of broad-band digital seismic stations in the Indian region recorded from events surrounding the continent to study the lateral heterogeneity in the crust and upper mantle. Previous surface wave studies carried out in peninsular India and the surrounding region include

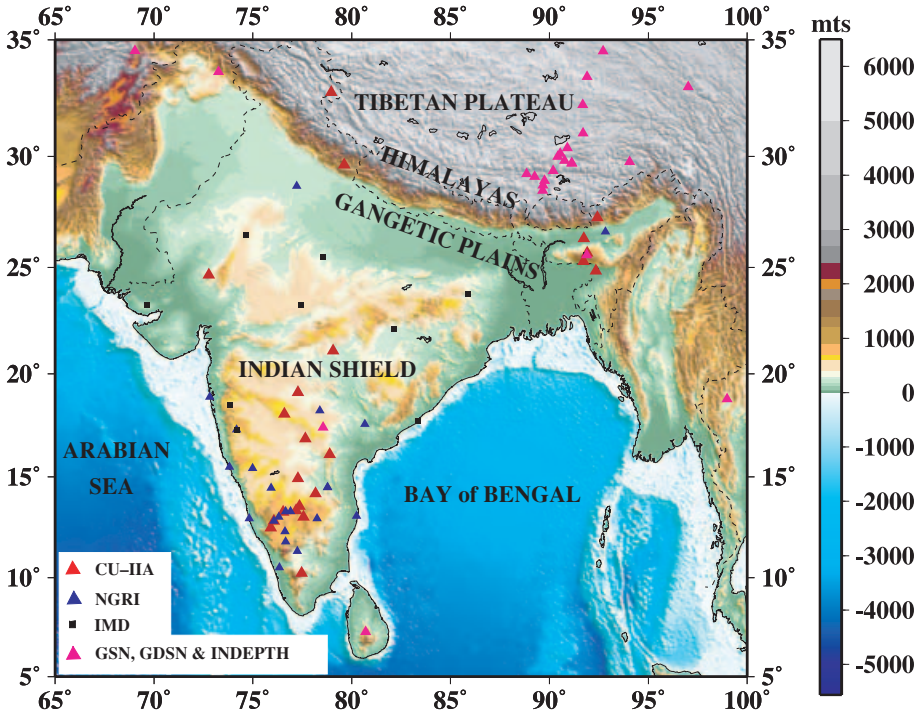

Figure 1. Map showing the different network stations, which recorded data for the dispersion study. The legend on the map indicates the different seismic networks.

those by Bhattacharya (1974, 1981), Brune & Singh (1986), Hwang & Mitchell (1987), Singh (1988), Mohan *et al.* (1992) and Singh *et al.* (1999). We discuss these results below and compare them with our new findings. We believe that the more detailed group velocity images of India presented in this paper are a significant improvement over published dispersion results for India and enhance the confidence with which its variegated terranes can be visualized.

2 DATA AND GROUP VELOCITY ANALYSIS

2.1 Data source

Data for this study come from both permanent and temporary seismic stations operating in the region. We obtained data from the IRIS data management centre for the permanent stations HYB (Geoscope), LSA (Chinese Digital Network), NIL and PALK (IRIS-IDA) and CHTO, KAAO and SHIO (US Geological Survey) and for the Tibet-PASSCAL (Owens *et al.* 1993) and INDEPTH-II (Yuan *et al.* 1997) PASSCAL experiments in Tibet (Fig. 1, Table 1). Most of the data for peninsular India comes from stations operated by the Indian Meteorological Department (IMD), the National Geophysical Research Institute (NGRI) and jointly by the Indian Institute of Astrophysics and the University of Cambridge (IIA-CU) (Fig. 1, Table 2). We analyse seismograms from these stations for 282 magnitude 4.9 and greater events, which occurred between 1975 and 2003. These provide 1001 source–receiver paths, which cover a wide range of azimuths and path lengths across the region, providing a dense sampling of southern Tibet, the Himalaya, the south Indian shield, the eastern Arabian Sea, and the Bay of Bengal (Fig. 2).

2.2 Group velocity determination

Our analysis proceeds in two stages:

(i) measurement of Rayleigh wave group velocity dispersion curves and their estimated errors along individual source–receiver paths, and

(ii) combination of the group velocity data to produce tomographic group velocity maps of the Indian shield at a number of periods ranging from 15 to 45 s.

In the first step of the analysis we use FTAN (Levshin *et al.* 1972, 1992) to isolate the desired part of the waveform from the seismogram so as to obtain an accurate estimate of the group velocity and its error bound for each source–receiver path. We first construct an energy *versus* period diagram of the surface wave part of the seismogram and manually trace the energy maximum of the fundamental mode Rayleigh wave. This curve is used to construct a time-variable filter (Herrin & Goforth 1986; Russell *et al.* 1988) whereby the desired fundamental mode surface wave signal can be extracted from the observed waveform consisting of body waves, higher modes and multipath surface waves, in addition to the desired fundamental mode Rayleigh wave. This results in an energy-period diagram, which is converted to group velocity using the earthquake epicentre and origin time taken from the Enghdal seismic catalogue. Location errors for this catalogue are less than ± 10 km and origin time errors of the order ± 2 s for this region (Enghdal, personal communications, 2004) resulting in a group velocity error of less than ± 0.02 km s^{-1} for our average path length. This procedure is applied to that part of the energy-period diagram where the high-energy ridge is clearly above the noise. We follow this procedure to measure the Rayleigh wave group velocity dispersion for the 1001 source–receiver paths (Fig. 2) and we then employ spline interpolation to obtain the group velocity at 15, 18, 20, 22, 25, 30, 35 and 45 s period.

Table 1. Location and seismometer type of GDSN, WWSSN, SRO-ASRO, PASSCAL, Geoscope and & II stations, which recorded data used in this study.

Network	Station	Latitude (°N)	Longitude (°E)	Elevation (m)	Seismometer type
CD	LSA	29.700	91.150	3789	STS-1
G	HYB	17.417	78.553	510	STS-1
II	PALK	07.272	80.702	460	STS-1
II	NIL	33.650	73.268	629	STS-1
IU	CHTO	18.790	98.977	316	STS-1
SR	CHTO	18.790	98.977	316	KS-36000
AS	KAAO	34.541	69.043	1920	KS-36000
SR	SHIO	25.566	91.883	1509	KS-36000
XC	AMDO	32.247	91.688	4712	STS-2
XC	ERDO	34.520	92.707	4623	STS-2
XC	GANZ	29.767	94.050	3150	STS-2
XC	LHSA	29.702	91.128	3700	CMG-3ESP
XC	SANG	31.024	91.700	4740	STS-2
XC	TUNL	36.199	94.815	3133	CMG-3ESP
XC	USHU	33.011	97.015	3727	STS-2
XC	WNDO	33.448	91.904	4865	STS-2
XC	XIGA	29.234	88.851	3865	STS-2
XR	BB05	30.3792	90.9108	4219	CMG-3T
XR	BB08	30.1301	90.5484	4361	CMG-3T
XR	BB10	29.9974	90.4142	4369	CMG-3T
XR	BB14	29.3682	90.1846	3792	CMG-3T
XR	BB18	28.9301	89.7440	4246	CMG-3T
XR	BB20	28.7274	89.6644	4245	CMG-3T
XR	BB23	28.4857	89.6585	4379	CMG-3T
XR	BB34	29.1077	89.2517	4002	CMG-3T
XR	BB36	29.8160	90.7570	3910	CMG-3T

2.3 Building the group velocity maps

In the second stage of the analysis we combined the individual path-averaged group velocity measurements to form tomographic group velocity maps at a number of discrete periods. To perform the tomographic inversion we follow Sambridge & Gudmundsson (1998) and parametrized the Indian region by a 2-D finite element mesh of triangular elements with sides of length 1° on a spherical surface. Each node point of the triangular mesh is described by a position vector from the centre of the Earth. We calculated the group slowness at the nodes of these triangles from intersecting propagation paths for which Rayleigh wave group velocity dispersion measurements were made. A three-point linear interpolation was used to evaluate the model within each triangular element in the gridded region. The data included in the analysis consisted of group traveltimes for the various earthquake-receiver paths. We assumed that surface waves propagate in an isotropic earth and follow the great circle path joining the earthquake and the receiver. The traveltime t for the path is

$$t = \int_{\text{path}} u\, dx \;=\; \sum_{i=1}^{n} \int_0^{l_i} u\, dx \tag{1}$$

where u is the slowness, l_i denotes the length of the ray path segment within the ith triangle, and the summation is over all triangles. Within each triangle, u at any given point $\mathbf{x}$ along the ray path is given by:

$$u \;=\; \varepsilon_0 u(\mathbf{x_0}) + \varepsilon_1 u(\mathbf{x_1}) + \varepsilon_2 u(\mathbf{x_2}), \tag{2}$$

where $\mathbf{x}_0$, $\mathbf{x}_1$ and $\mathbf{x}_2$ are the position vectors of the triangle node points and ε_0, ε_1, ε_2 are the weights assigned to the three nodes with $\varepsilon_0 + \varepsilon_1 + \varepsilon_2 = 1$. Substituting eq. (2) in eq. (1) gives

$$t \;=\; \sum_{i=1}^{n} \left[u(\mathbf{x_0}) \int_0^{l_i} \varepsilon_0\, dx + u(\mathbf{x_1}) \int_0^{l_i} \varepsilon_1\, dx + u(\mathbf{x_2}) \int_0^{l_i} \varepsilon_2\, dx \right] \tag{3}$$

Summing over the node points of the triangles, eq. (3) can be rewritten:

$$t \;=\; \sum_{\text{points}} u(x) \sum_{\text{triangles}} \int \varepsilon\, dx. \tag{4}$$

The forward problem can then be expressed by:

$$\mathbf{d} = [G]\ \text{x}\ \mathbf{m}, \tag{5}$$

where $\mathbf{d}$ is the N-dimensional vector of traveltime data t, $\mathbf{m}$ is an M-dimensional vector of the slowness values at the nodes, and $[G]$ is the operator that maps vectors in the model space into vectors in the data space. The construction of the specific form of $[G]$ used in this study is given in Mitra (2004). We solve eq. (5) for the model vector $\mathbf{m}$ by minimizing the sum of the data-weighted sum of squares and the smoothed sum of squares for the model vector, formulated as

$$\text{data sum of squares} \;=\; (\mathbf{d} - G\mathbf{m})^T V^{-1} (\mathbf{d} - G\mathbf{m})$$

$$\text{smoothed sum of squares} \;=\; \mathbf{m}^T V_s^{-1} \mathbf{m},$$

where V is the data variance matrix and V_s is the variance matrix associated with the *a priori* probability constraints on the model vector $\mathbf{m}$. The *a priori* constraints used constitute the differences between values of the model parameter (i.e. slowness) at different node points in the triangular grid and do not significantly affect the overall average value of slowness determined from the data. The resulting model vector $\mathbf{m}$ is

$$\mathbf{m} = (V_s^{-1} + G^T V^{-1} G)^{-1} G^T V^{-1} \mathbf{d}, \tag{6}$$

where the term in brackets is the *a posteriori* variance matrix. We have followed this procedure to build Rayleigh wave group velocity maps for India and the surrounding region at 15–45 s period.

Table 2. Location and seismometer type of NGRI, IMD and CU-IIA stations which recorded data used in this study.

Network	Station	Latitude (°N)	Longitude (°E)	Elevation (m)	Seismometer type
NG	MTP	11.32	77.25	321	CMG-3ESP
NG	BGL	13.021	77.570	791	CMG-3ESP
NG	TPT	13.274	76.536	785	CMG-3ESP
NG	GBA	13.564	77.357	681	CMG-3ESP
NG	KDR	14.176	78.164	453	CMG-3ESP
NG	LTV	14.927	77.281	396	CMG-3ESP
NG	DHR	15.43	74.98	682	CMG-3ESP
NG	SLM	16.101	78.894	368	CMG-3ESP
NG	KIL	18.069	76.598	522	CMG-3ESP
NG	TEZ	26.633	92.833	69	CMG-3ESP
SE	GOA	15.491	73.824	58	CMG-40T
SE	BOM	18.895	72.812	6	CMG-40T
SE	TRV	8.510	76.960	64	STS-2
SE	MNG	12.941	74.822	11	CMG-40T
SE	MDR	13.070	80.250	15	STS-2
SE	PUNE	18.530	73.850	560	STS-2
SE	NGP	21.101	79.062	304	CMG-40T
SE	JHN	25.465	78.539	250	CMG-40T
SE	SHL	25.566	91.855	1600	CMG-40T
SE	NDI	28.683	77.216	219	CMG-40T
SE	KARD	17.307	74.183	561	STS-2
SE	VISK	17.721	83.328	10	STS-2
SE	BLSP	22.129	82.131	271	STS-2
SE	BHPL	23.241	77.424	502	STS-2
SE	BHUJ	23.254	69.654	101	STS-2
SE	BOKR	23.794	85.885	307	STS-2
SE	AJMR	26.479	74.643	492	STS-2
CU	KOD	10.231	77.465	2258	CMG-3T
CU	KSL	12.49	75.91	877	CMG-3T
CU	GRR	12.827	76.062	792	CMG-3T
CU	HSN	12.827	76.062	792	CMG-3T
CU	CRP	13.02	76.32	894	CMG-3T
CU	TMK	13.343	77.194	842	CMG-3T
CU	MBN	16.871	77.657	417	CMG-3T
CU	NND	19.107	77.287	314	CMG-3T
CU	ABU	24.653	72.779	1431	CMG-3T
CU	KMG	24.846	92.343	18	CMG-3T
CU	CHP	25.280	91.723	1312	CMG-3T
CU	BPN	25.669	91.908	951	CMG-3T
CU	BAI	26.318	91.739	99	CMG-3T
CU	BMD	27.271	92.418	2792	CMG-3T
CU	ALM	29.637	79.620	1188	CMG-3T
CU	HNL	32.778	78.973	4284	CMG-3T

2.4 Reliability of the group velocity maps

Before discussing the significance of the variations shown in our tomographic group velocity maps, we evaluate the reliability of the group velocity images. Uncertainties arise mainly from measurement errors in the group velocity for individual paths, which result from errors in the hypocentral parameters for the earthquakes and from noise in the data, and in the tomographic maps from poor ray path coverage. The former have been taken into account by estimating the uncertainty in measurements for every path; however, the latter is dependent on the path distribution and can be evaluated by standard checkerboard tests. For a given choice of *a priori* slowness in the inversion, the path density, average path lengths and azimuthal distribution control the resolution of the model.

The effects of smearing of features along ray paths when insufficient ray crossings are available are well recognized. Formal resolution parameters for tomographic models are not often determined because of the size of the computational problem. The usual approach is to estimate resolution by inverting synthetic data for a simple velocity model; the similarity of the synthetic input model and inversion output image is then taken as an estimate of the data resolution. It is generally accepted that if the inversion of the synthetic data can retrieve small-scale structures in, for example, a checkerboard test, then large-scale structures will be well resolved. However, Lévêque *et al.* (1993) have shown that this is not necessarily true, and that such synthetic experiments can be misleading. They use simple models to demonstrate that large-scale structures are not always more easily retrieved than are small-scale structures. Therefore, we perform a series of checkerboard tests to estimate the resolution of the group velocity images. We constructed three checkerboard input models with square cells of sides 5°, 7.5° and 10°, each being parametrized as alternate high and low velocities of 2.5 km s^{-1} and 4 km s^{-1}, respectively. We calculate the group traveltimes for each path through these velocity models and invert the synthetic group traveltimes using the same *a priori* slowness employed in the analysis of the real data.

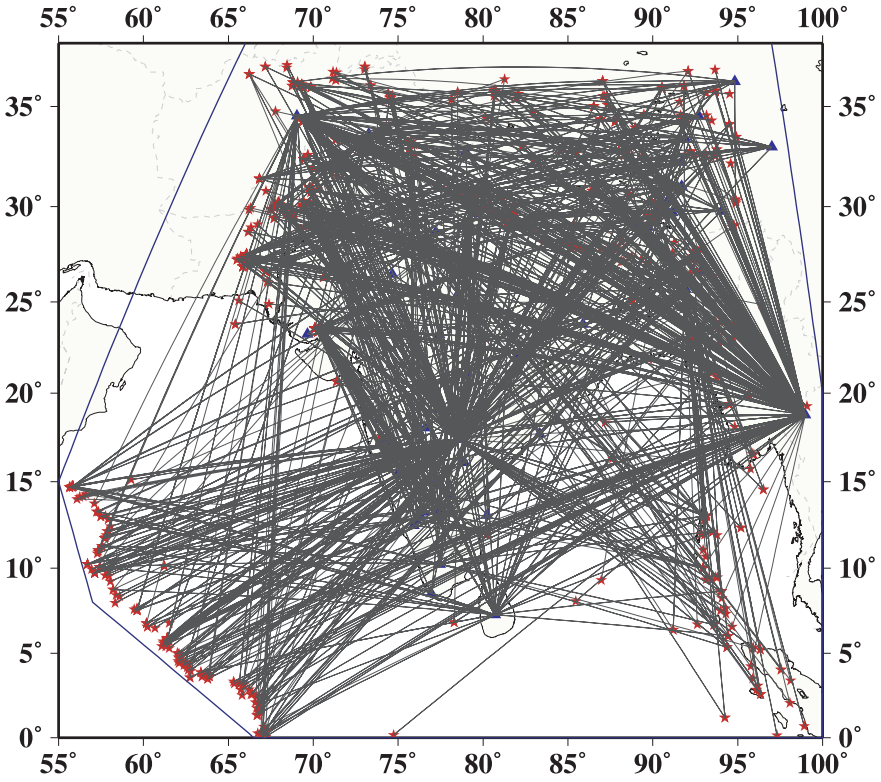

Figure 2. Source–receiver ray path coverage map for the complete dataset used in the analysis. The average source–receiver path length is about 10°.

We plot the checkerboard recovery map for 20 s period with the original input model for the three cell sizes in Fig. 3. The spatial pattern is well resolved over peninsular India for the 5° checkerboard map, but the amplitude is underestimated. The best resolution of the 5° checkerboard is for the southern and eastern part of India and the northern Bay of Bengal. Both the spatial pattern and amplitudes are well resolved for the 10° checkerboard except for the Arabian Sea region, where the paths are mostly in the SW–NE direction with only a few intersecting N–S paths. The resolution of the 7.5° checkerboard is not significantly worse that the resolution of the 10° checkerboard. In presenting our results we have plotted the 7.5° checkerboard resolutions for each period to indicate the resolved features in the tomographic images at each period.

We have not considered the effects of azimuthal anisotropy in the group velocity maps. Pilidou *et al.* (2005) show from synthetic tests that for the velocity structure, there can be 1–2 per cent trade-off between azimuthal anisotropy and shear wave speed heterogeneity.

3 GROUP VELOCITY MAPS

The Rayleigh wave group velocity maps at 15, 18, 20, 22, 25, 30, 35, 40 and 45 s period are plotted in Figs 4–6. Calculations were made for *a priori* slowness standard deviation values ranging from 0.001 to 0.5. Increasing the *a priori* slowness standard deviation enhances details in the tomographic image because of the larger range of variation allowed in the slowness calculations; however, this accentuates the errors, whereas a decrease in the *a priori* slowness results in greater smoothing of the solution space and decrease in errors. The group velocity maps shown in Figs 4–6 were calculated using an *a priori* slowness standard deviation of 0.045 for a reference distance of 10°. This choice was made by examining the trade-off between the misfits, the smoothness, and the features of the resulting group velocity maps. We empirically test that the overall average value of the slowness determined from the data does not change with the choice of the *a priori* smoothness value. Our final group velocity maps are contoured at 0.1 km s^{-1} intervals. We have clipped areas of the maps with errors larger than 0.15 km s^{-1}. This error cut-off understandably matches regions with poor data coverage. This choice of masking is subjective; however, we have plotted the 7.5° checkerboard results for each period in Figs 4–6 so the resolution can be independently judged.

Because of the large number of seismograms used from seismographs located in peninsula India, these results provide better lateral resolution over the Indian peninsular region compared to published global (Larson & Ekstrom 2001) and regional (Ritzwoller & Levshin 1998) group velocity studies. The depth of sampling of Rayleigh waves increases with increasing period and at a particular period, the group velocity is related to an integrated average of velocities to a wavelength-dependent depth. In view of this, we draw correlations between the surface wave velocity heterogeneity in the Indian region and its broad tectonic and geological features. The maps at shorter periods (15–22 s) are primarily influenced by the upper crust; periods (25–35 s) are principally influenced by the lower crust, while the longer periods probe the lower crust and uppermost-mantle structure beneath the region. The most distinctive feature across the entire period range of measurements is the consistent difference between south India, which is characterized by higher group velocities at all periods, and north India and southern Tibet, which are characterized by lower group velocities at all periods. Much of this difference is related to the thick sediment in the Ganges Basin and the extremely thick crust in southern Tibet.

The high-frequency maps (Figs 4 and 5) show that the northern Bay of Bengal has the slowest velocities (∼2 km s^{-1}) in the whole region, with a marked positive velocity gradient towards the south.

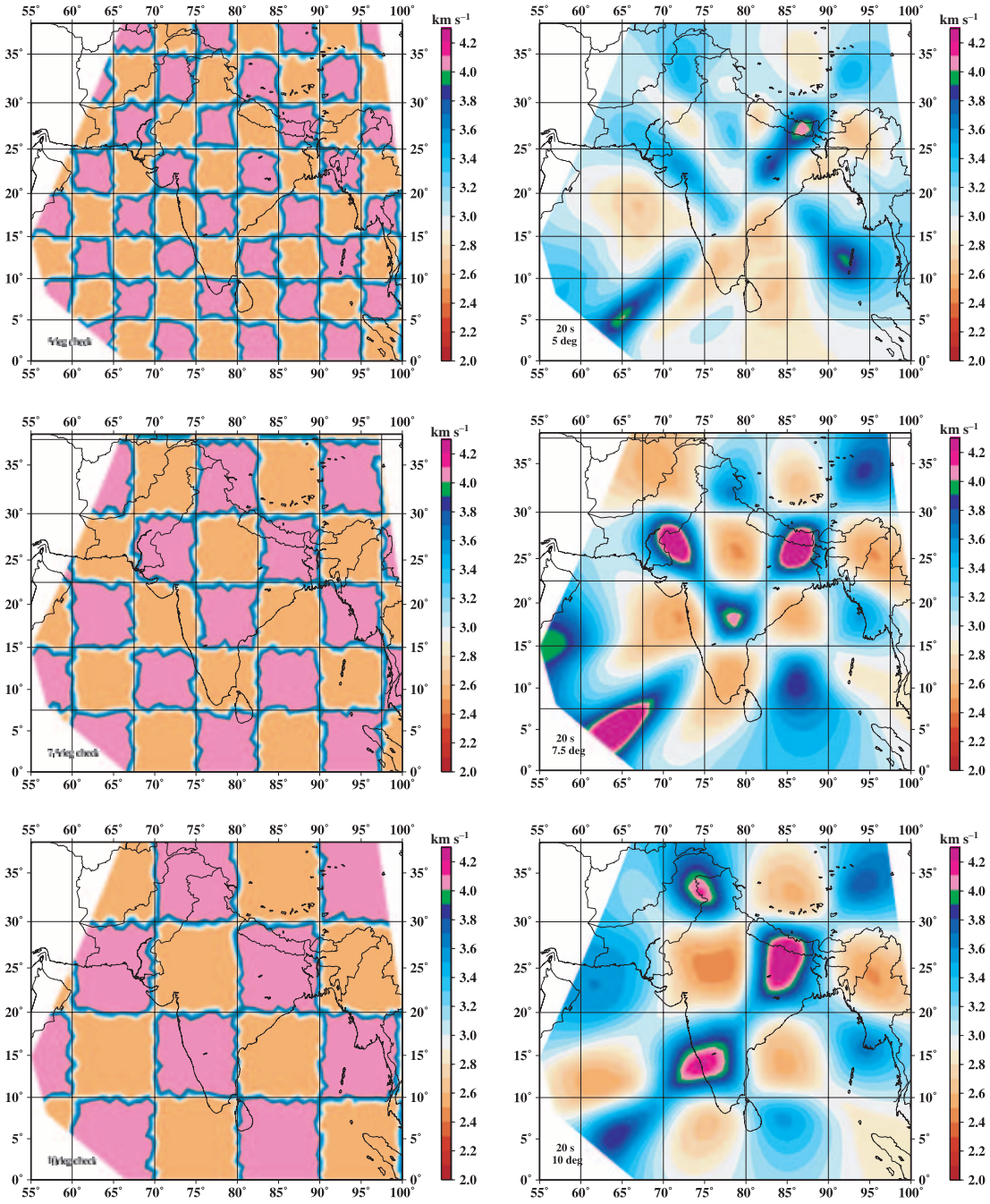

Figure 3. Checkerboard tests for ray coverage at 20 s period. On the left are the input checkerboards for cell sizes 5°, 7.5° and 10°. On the right are the recovered velocities for the given ray coverage and cell size. The uneven edges of the checker result from the triangular parametrization.

At 15 s period (Fig. 4b) the low velocity in the Bay of Bengal lies along the Andaman arc region. The velocity gradient in the western Bay of Bengal conforms to the continental margin with higher velocities across the eastern coast of India. In the southern Bay of Bengal to the east of Sri Lanka, a NS-elongated high-velocity zone exists, which subsequently (30 s period map, Fig. 5f) becomes a high-velocity domal structure. South and central India are marked by a high-velocity centre, elongated in an EW direction (Fig. 4b). The higher velocities also extend towards northwestern India. The Gangetic plains show relatively low velocities with gradients to even lower values at 20 s period (Fig. 4f) beneath the central Himalaya. The Himalayan arc displays overall lower velocities compared to the Indian shield region, although a high-velocity centre is seen beneath the NE syntaxial bend of the Himalaya and the Shillong Plateau region (Figs 4b, d, f and 5b, d). This delineates an interesting velocity transition from the central Himalayan arc towards the NE bend, ranging from low-to-high group velocity (2.8–3.3 km s^{-1}) within a span of a few hundred kilometres. The Tibetan Plateau north of the Himalaya is characterized by low velocities (Figs 4b, d, f and 5b, d, f). Extremely low velocities occur in central Pakistan with a southward gradient towards the Arabian Sea (Fig. 4b) similar to the velocities and structure in the Bay of Bengal. Finally, the southwestern Arabian Sea is marked by the highest velocities in the region although this is on the border of our maps.

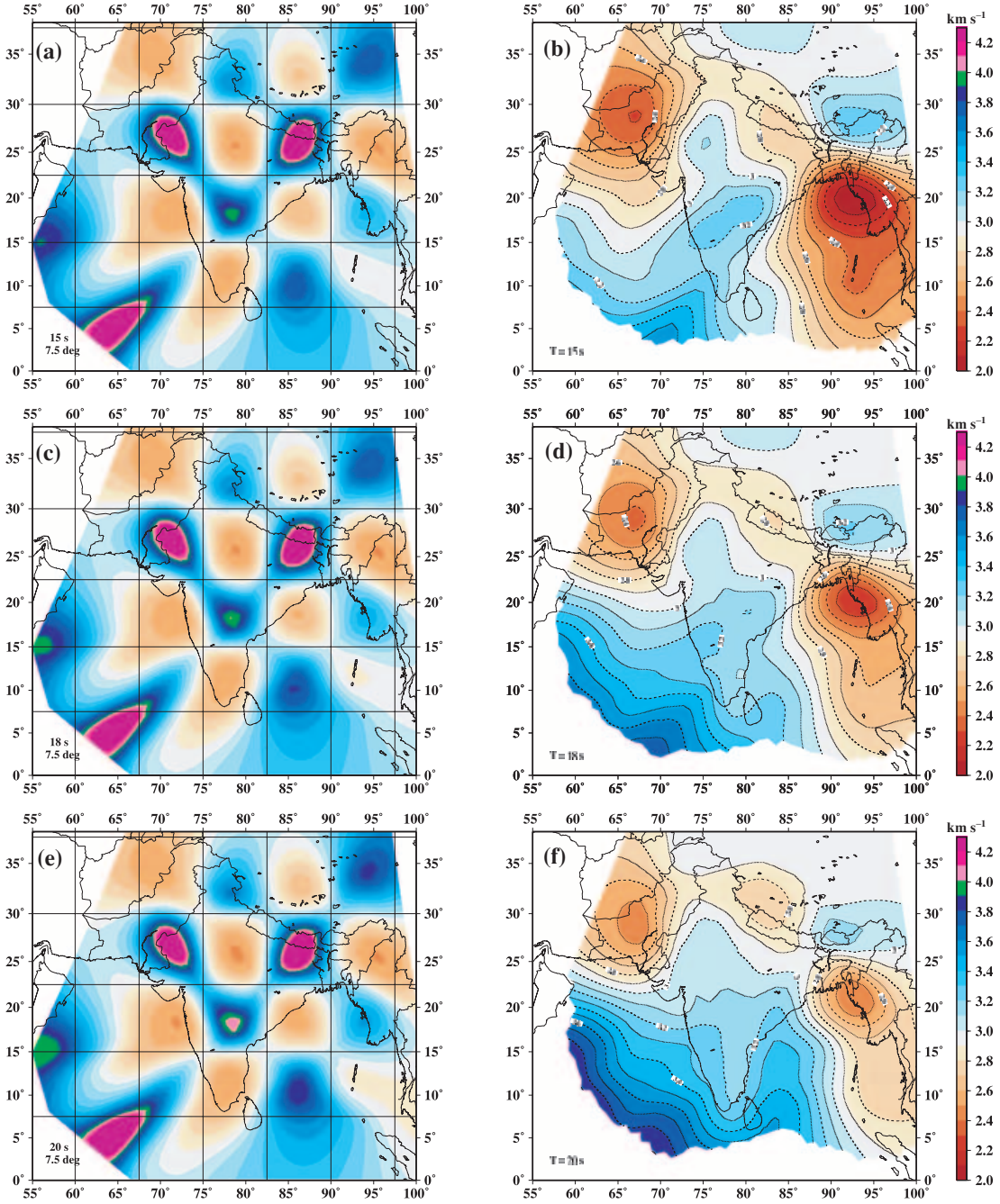

Figure 4. Rayleigh wave group velocity tomography map at 15, 18, and 20 s period. On the left (a, c and e) are the checkerboard test images for the 7.5° grid to provide a guide for the regions best resolved by the tomographic inversion at a given period. On the right (b, d and f) are the tomographic images. The red colour indicates slower velocities (<3 km s^{-1}) while the blue–pink regions have faster velocities (>3 km s^{-1}) (see scale). The contour interval on the tomographic maps is 0.1 km s^{-1} with the contours labelled every 0.2 km s^{-1}. Regions with errors greater than 0.15 km s^{-1} are clipped.

At longer periods (35–45 s maps, Fig. 6), the general difference between southern and northern India, that is, higher group velocities in the south and lower in the north are preserved. The high velocities seen in the southern Bay of Bengal at short periods spread northwards (Figs 6b and d). The high velocity around the NE syntaxis of the Himalaya diminishes and the whole of the Himalayan arc is bounded by the high velocity gradient to the south. The Tibetan Plateau shows lower velocities, which are confined to the central part of the Plateau at our longest periods. The lower velocities in Pakistan persist to 45 s and the high velocities in the Arabian Sea that are seen at shorter periods continue at longer periods.

4 DISCUSSION AND GEOLOGICAL CORRELATION

Fig. 7 compares the 15 s tomographic map with the geological map of India in order to draw a correlation between the lateral velocity variations and the corresponding geological and tectonic units. We have selected the 15 s map for this illustration because it samples

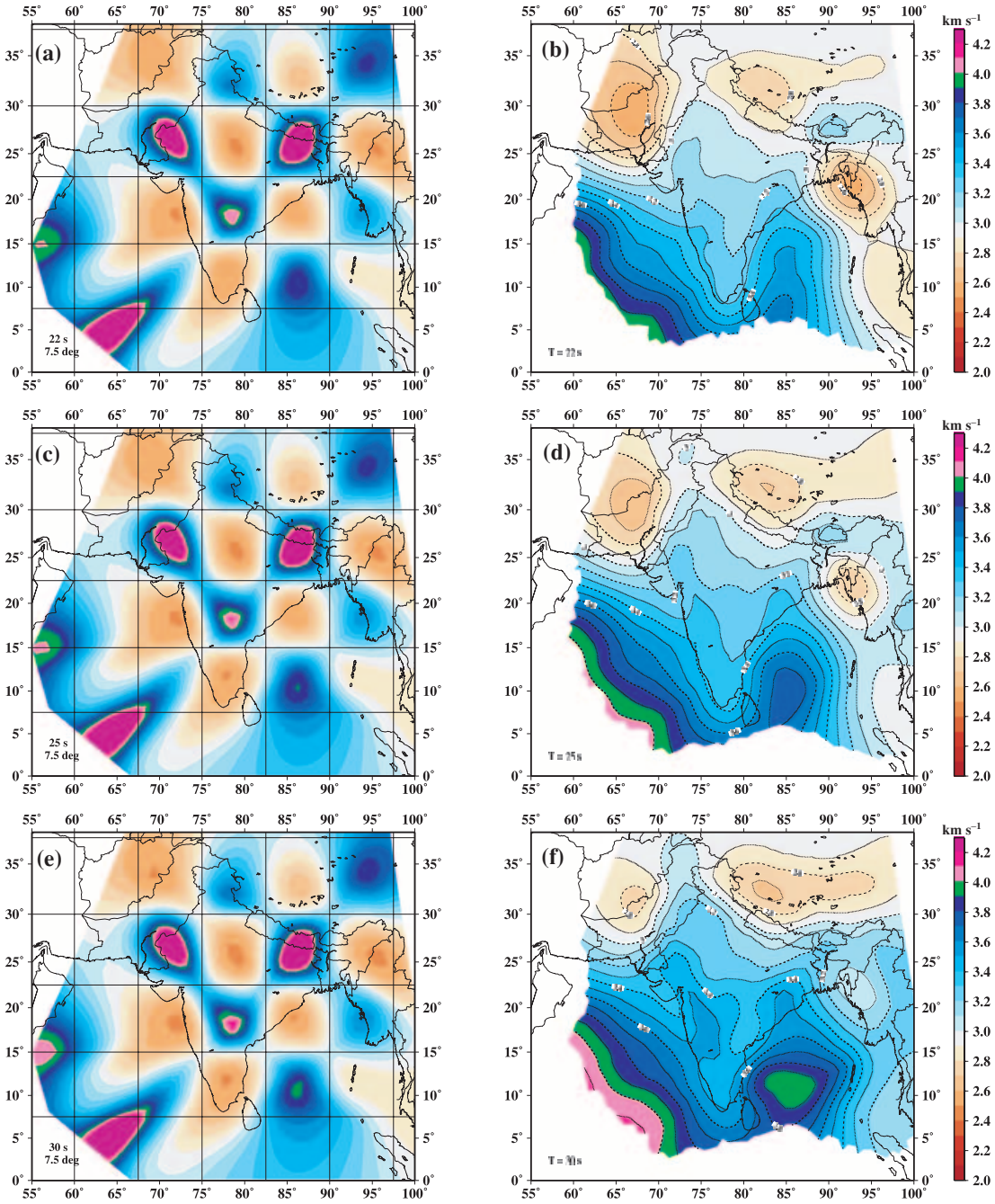

Figure 5. Tomography map at 22, 25 and 30 s period. The figure format is the same as for Fig. 4.

the shallow crustal structure and is, therefore, more meaningful in correlating with surface geology (Fig. 7a).

The Precambrian shield region of southern and central India corresponds to high velocities in the tomographic image. Since the mobile belts between the cratons are too narrow to be resolved, the tomographic images of the Dharwar and the Singhbhum Cratons appear to have merged to form an eastward-elongated high-velocity region in the south. Its further extension northwards conforms to the Proterozoic Aravali Craton. These high cratonic velocities persist at longer periods and to somewhat longer periods for the Dharwar Craton (Figs 6b, d and f) than for the Singhbhum or Aravali Cratons. The low velocity at 15 s period beneath the Gangetic Plains results from the mollasse sediments in the Himalayan foredeep overlain by recent alluvium. At longer periods (30–45 s) high group velocities occur beneath the Ganges Plain as the longer period waves sense the downwarpped crystalline crust below the sediments. The northern Bay of Bengal, which has the slowest velocities, has the thickest pile of basin sediments (∼22 km in the north) transported from the Himalaya by the Ganges and the Brahmaputra Rivers (Curray *et al.* 1982; Brune & Singh 1986), the sediment cover thinning southeast towards the distal part of the fan. Thus, this low-velocity region is a map of the subareal delta of the Ganges and Brahmaputra Rivers and the submarine Bengal fan. The geometry of the fan closely matches the gradient of the low-velocity image and the contouring of this low velocity SE along the Andaman Islands may reflects the sediment infill of the trench-arc structure.

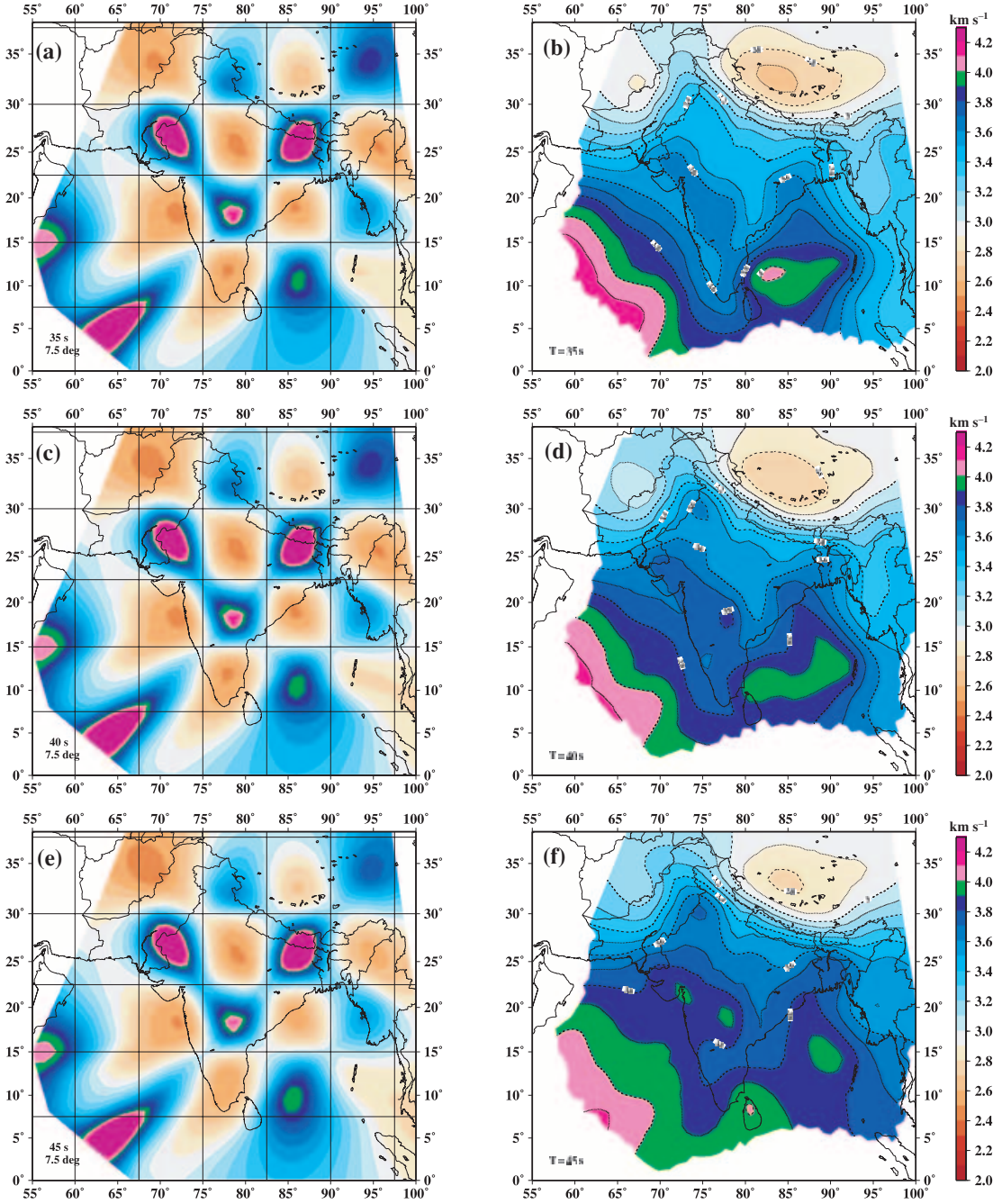

Figure 6. Tomography map at 35, 40 and 45 s period. The figure format is the same as for Fig. 4.

Similar low velocities in the NW conform to the Katawaz Basin in Pakistan, which evolved in the Tertiary as a remnant of the Neo-Tethys Ocean basin before the collision of the western passive margin of the Indian subcontinent (including Pakistan) with the Afghanistan block (Qayyum *et al.* 1996). The Basin is filled with about 8 km of Tertiary sediments deposited in the Khojak submarine fan (a palaeocounterpart of the Indus fan) overlain by late-stage mollasse sediments. The southward velocity gradient conforms to the present submarine Indus fan which progrades into the Arabian Sea, being fed by the sediment derived from the northwestern Himalaya at the headwaters of the Indus River. The NW–SE-striking low-velocity zone along the Himalayan arc at 15 and 18 s (Figs 7 and 4d) is an image of the collision zone. At longer periods (20–40 s) this low-velocity zone localizes to a low-velocity oval beneath the central Himalaya (Figs 5 and 6), corresponding to thicker crust beneath the fold-and-thrust belt. At 35–45 s period the low velocity moves northwards towards the Tibetan Plateau where the Indian plate underthrusts the Eurasian plate. Here the tomographic images reveal crustal doubling (80–90-km-thick crust) (Yuan *et al.* 1997; Mitra *et al.* 2005). The high velocity observed around the NE syntaxial bend of the Himalaya and the Shillong Plateau does not match the surface geology, but exhibits a possibly colder lower-crust beneath the region and corroborates previous findings (Mitra *et al.* 2005) of the whole crust being seismically active. The other striking feature

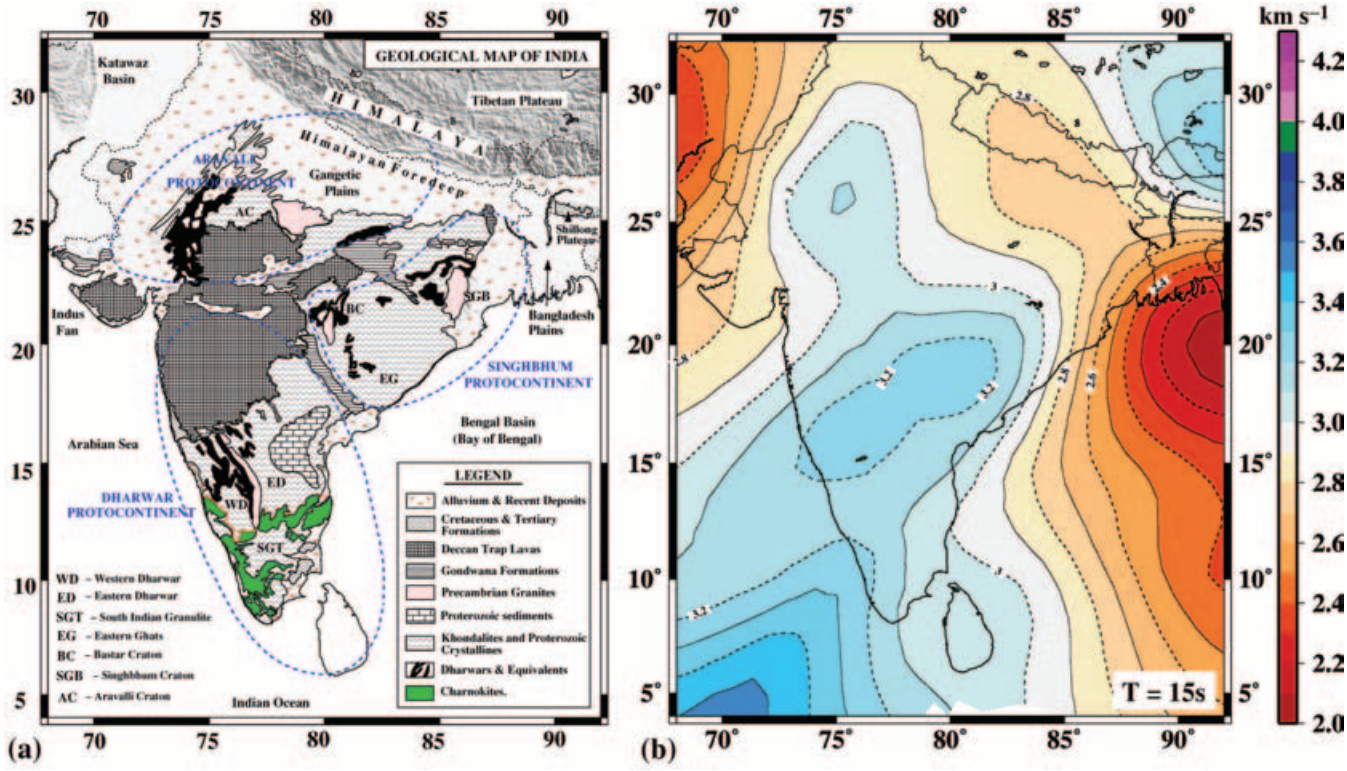

Figure 7. A comparative plot of (a) the geological map of India with (b) the tomographic image at 15 s period.

is the high-velocity domal structure in the southern Bengal Basin which, if traced on subsequent frequency images (starting from 20 s), could be the manifestation of the 85°E ridge in the Indian Ocean (Liu *et al.* 1982). The higher velocities in the SW Arabian Sea constitute an image of the oceanic crust and upper mantle but in this region our path coverage is poorest.

Thus, the transition boundary between the higher and lower velocities in the higher-frequency maps conforms well with the Indian cratonic regions and the surface geology. The difference in group velocities over the Indian shield region diminishes as we go to lower frequencies, but the overall disparity in velocity between the shield region and the Himalayan arc is maintained even at longer periods. At these lower frequencies the Rayleigh wave maps are, to a first order, inversely related to the Moho depth (Ritzwoller & Levshin 1998), that is, the low velocities result largely from thickened crust. Hence, the overall high velocity in the Indian shield at lower frequencies (Fig. 6) images the high-velocity root typical of shield regions. The lateral resolution becomes marginally poorer at lower frequencies due to fewer ray paths.

Previous surface wave dispersion studies of the Indian region were severely limited by the number of seismographs in India yielding lower resolution images. Bhattacharya (1974,1981) measured group and phase velocity dispersion to 100 s period along a few paths crossing the Indian Peninsula to determine its upper mantle structure. These showed that shield-like crustal velocities extended below the sediments of the Himalayan foredeep in northern India. Our group velocity maps confirm this earlier observation. Hwang & Mitchell (1987) determined fundamental mode Rayleigh wave group velocity for periods between 2 and 90 s for 14 paths across the Indian Peninsula and for periods between 4 and 40 s for 10 Himalayan paths. For both regions the group velocities show small scatter at longer periods (>30 s) but larger scatter at short periods (<20 s). Their average group velocity curves for both regions fall within the range of group velocities we observe where the period ranges of the two studies overlap. Hwang & Mitchell (1987) invert their dispersion data and obtain a simple shear wave model for the Indian shield consisting of a gradational crust with a velocity increasing from ∼3.5 km s^{-1} at the surface to ∼4.0 km s^{-1} at the base of the crust. Their inversion of the Himalaya dispersion data indicates a 55-km-thick crust consisting of 30-km-thick upper crust (∼3.4 km s^{-1}) and a 25-km-thick lower crust (∼3.8 km s^{-1}) overlying a low velocity (∼4.4 km s^{-1}) upper mantle.

Mohan *et al.* (1992) determined Rayleigh wave group velocity over the Indian region for periods from 15 to 60 s for 63 paths across the Arabian Sea, the Bay of Bengal, the Indian Peninsula and the Himalaya to produce sparse group velocity maps. Although they are much less detailed compared to the group velocity maps presented in this study, the maps of Mohan *et al.* (1992) do show the divide between low group velocities in the Himalaya and Gangetic plane in the north and the high group velocities in the Indian shield to the south, consistent with our group velocity maps. Singh *et al.* (1999) used recordings of the 1997 May 21 Jabalpur earthquake at 10 broad-band IMD seismographs and three additional recordings at HYB to determine fundamental mode Rayleigh and Love wave group velocity dispersion in the period range 10–75 s for paths over southern India. These same seismograms, which gave similar group velocities, have been incorporated into our group velocity analysis. Singh *et al.* (1999) inverted their group velocity data for a simple crustal model for central India consisting of a 14-km-thick, 3.55 km s^{-1} upper layer, a 25-km-thick, 3.85 km s^{-1} lower layer overlying a 4.65 km s^{-1} upper mantle.

Brune & Singh (1986) measured fundamental mode Rayleigh wave group velocities from seismograms recorded at sites in eastern India from events in the Andaman arc. They found extremely low group velocities (< 2 km s^{-1} at 20 s period) for paths crossing the northern part of the Bay of Bengal but more normal group velocities ($\sim$3.5 km s^{-1} at 20 s period) for paths crossing the southern part of the Bay. They inverted fundamental and higher mode surface wave dispersion data for discrete paths across the Bay of Bengal and found an increasing crustal thickness from $\sim$15 km at the latitude of the southern tip of India to $\sim$35 km at the northern end of the Bay of Bengal, the sedimentary cover increasing from $\sim$8 km in the south to over 15 km in the northern part of the Bay. Singh (1988) made similar measurements for paths crossing the Arabian Sea to the west of India and found somewhat higher group velocities for paths crossing the Indus fan in the Arabian Sea compared to group velocities for paths crossing the Ganges–Brahmaputra fan in the Bay of Bengal. He interpreted these dispersion data as indicating that the subsediment crystalline crust increased in thickness from 16 km to the west of the tip of southern India to 28 km beneath the northern part of the fan. The sediment thickness increased from $\sim$7 km along his southernmost paths to $\sim$10 km along his northernmost paths.

There have been a large number of surface wave dispersion studies of the Tibetan Plateau, but most of the early results were from analyses of seismograms recorded at stations outside Tibet. The recent study of Rapine *et al.* (2003) analyses seismograms for paths confined to the Plateau and finds fundamental mode Rayleigh wave group velocities less than 3 km s^{-1} between 15 and 45 s period, similar to the low group velocities we observe in southern Tibet. Rapine *et al.* (2003) invert their group velocity data for southern Tibet and find that a mid-crustal low-velocity zone is required by these observed low group velocities.

5 CONCLUSION

We have calculated Rayleigh wave group velocity dispersion over the Indian region using a dense ray path coverage and combined our path-averaged measurements to create a series of tomographic images of group velocity variations over the region at periods of 15–45 s. Our study yields a significant improvement over the previous work done on surface wave dispersion in India because of:

(i) denser and more uniform data coverage;

(ii) higher resolution of the tomographic images compared to previous studies performed on this scale and

(iii) consistency with which the group velocity maps image the known geological and tectonic features of the region, either mapped at the surface or inferred at depths. The high-frequency maps provide tighter constraints on lateral velocity variations in the crust and image with good resolution the Archean–Proterozoic stable cratons, thick sedimentary basins and the Himalayan fold and thrust belt. The lower frequency maps resolve the thicker crust beneath the fold and thrust belt and crustal doubling beneath the Tibetan Plateau. They also image the upper portions of the high-velocity roots beneath the stable shields.

ACKNOWLEDGMENTS

VKG acknowledges the invaluable support provided by the Directors of the Indian Institute of Astrophysics and of C-MMACS, Bangalore.

REFERENCES

Bhattacharya, S., 1974, The crust-mantle structure of the Indian Peninsula from surface wave dispersion, *Geophys. J. R. Astr. Soc.,* **36,** 273–283.

Bhattacharya, S., 1981, Observation and inversion of surface wave group velocities across central India, *B. Seismol. Soc. Am.,* **71,** 1489–1501.

Brune, J. & Singh, D., 1986, Continent-like crustal thickness beneath the Bay of Bengal sediments, *B. Seismol. Soc. Am.,* **76,** 191–203.

Curray, J., Emmel, F., Moore, D. & Raitt, R., 1982, Structure, tectonics, and geological history of the northeastern Indian ocean, in *The Ocean Basins and Margins*, Vol. 6, pp. 399–450, eds Nairn, A. & Stehli, F , Plenum Publishing, New York.

Herrin, E. & Goforth, T., 1986, Phase-analysis of Rayleigh-waves from the Shagan River test site in the USSR, *B. Seismol. Soc. Am.,* **76,** 1739–1754.

Hwang, H.-J. & Mitchell, B., 1987, Shear velocities, q_β, and the frequency dependence of q_β in stable and tectonically active regions from surface wave observations, *Geophys. J. Int.,* **90,** 575–613.

Larson, E. & Ekstrom, G., 2001, Global models of surface wave group velocity, *Pure appl. Geophys.,* **158,** 1377–1399.

Lévêque, J.-J., Rivera, L. & Wittlinger, G., 1993, On the use of the checkerboard test to assess the resolution of tomographic inersions, *Geophys. J. Int.,* **115,** 313–318.

Levshin, A., Pisarenko, V. & Pogrebinsky, G., 1972, On a frequency-time analysis oscillations, *Annales Geophysicae,* **28,** 211–218.

Levshin, A., Ratnikova, L. & Berger, J., 1992, Peculiarities of surface-wave propagation across central Eurasia, *B. Seismol. Soc. Am.,* **82,** 2464–2493.

Liu, C., Sandwell, D. & Curray, J., 1982, The negative gravity field over the 85°e Ridge, *J. geophys. Res.,* **87,** 148–227.

Mitra, S., 2004, Crustal structure of NE India and southern Tibet and a comparison with the lithosphere of the stable Indian Shield, *PhD thesis,* University of Cambridge, Cambridge.

Mitra, S., Priestley, K., Bhattacharyya, A. & Gaur, V., 2005, Crustal structure and earthquake focal depths beneath northeastern India and southern Tibet, *Geophys. J. Int.,* **160,** 227–248.

Mohan, G., Rai, S. & Panza, G., 1992, Seismic heterogeneities in the Indian lithosphere, *Phys. Earth planet. Inter.,* **73,** 189–198.

Naqvi, S. & Rogers, J., 1987, *The Precambrian Geology of India,* Oxford University Press Inc, USA.

Owens, T., Randall, G., Wu, F. & Zeng, R., 1993, Passcal instrument preformance during the Tibet Plateau seismic experiment, *B. Seismol. Soc. Am.,* **83,** 1959–1970.

Pilidou, S., Priestley, K., Gudmundsson, G. & Debayle, E., 2005, Upper mantle S-wavespeed heterogeneity beneath the North Atlantic from regional surface waveform tomography: high resolution image of the Iceland plume, *Geophys. J. Int.,* **159,** 1057–1076.

Qayyum, M., Niem, A. & Lawrence, R., 1996, Newly discovered Paleogene deltaic sequence in Katawaz Basin, Pakistan, and its tectonic inplications, *Geology,* **24,** 835–838.

Rapine, R., Tilmann, F., West, M. & Ni, J., 2003, Crustal structure of northern and southern Tibet from surface wave dispersion analysis, *J. geophys. Res.,* **108,** doi:10.1029/2001JB000445.

Ritzwoller, M. & Levshin, A., 1998, Eurasian surface wave tomography: group velocities, *J. geophys. Res.,* **103,** 4839–4878.

Russell, D., Herrmann, R. & Hwang, H., 1988, The geology of the Persian Gulf—Gulf of Oman region: a synthesis, *B. Seismol. Soc. Am.,* **78,** 339–354.

Sambridge, M. & Gudmundsson, O., 1998, Tomographic systems of equations with irregular cells, *J. geophys. Res.,* **103,** 773–781.

Singh, D., 1988, Quasi-continental oceanic structure beneath the Arabian fan, sediments from observed surface-wave dispersion studies, *B. Seismol. Soc. Am.,* **78,** 1510–1521.

Singh, S., Dattatrayam, R., Shapiro, N., Mandal, P., Pacheco, J. & Midha, R., 1999, Crustal and upper mantle structure of peninsular India and source parameters of the 21 May 1997, Jabalpur earthquake (Mw = 5.8): results from a new regional broadband network, *B. Seismol. Soc. Am.,* **89,** 1631–1641.

Yuan, X., Ni, J., Kind, R., Mechie, J. & Sandvol, E., 1997, Lithospheric and upper mantle structure of southern Tibet from a seismological passive source experiment, *J. geophys. Res.,* **102,** 27 491–27 500.